Chinese Chemical Letters 34 (2023) 107405

Contents lists available at ScienceDirect

Chinese Chemical Letters

journal homepage: www.elsevier.com/locate/cclet

Ultrafine RuO_2 nanoparticles/MWCNTs cathodes for rechargeable Na-CO_2 batteries with accelerated kinetics of Na_2CO_3 decomposition

Zhenzhen Wang, Yichao Cai, Youxuan Ni, Yong Lu, Liu Lin, Haoxiang Sun, Haixia Li, Zhenhua Yan, Qing Zhao*, Jun Chen

Haihe Laboratory of Sustainable Chemical Transformations, Key Laboratory of Advanced Energy Materials Chemistry (Ministry of Education), Renewable Energy Conversion and Storage Center (RECAST), College of Chemistry, Nankai University, Tianjin 300071, China

ARTICLE INFO

Article history:
Received 5 March 2022
Revised 26 March 2022
Accepted 2 April 2022
Available online 5 April 2022

Keywords:
Na-CO_2 batteries
Cathode catalyst
RuO_2@a-MWCNTs
High rate performance
Low charge overpotential

ABSTRACT

Na-CO_2 batteries have attracted extensive attention due to their high theoretical energy density (1125 Wh/kg), efficient utilization of CO_2, and abundant sodium resources. However, they are trapped by the sluggish decomposition kinetic of discharge products (mainly Na_2CO_3) on cathode side during the charging process. Here we prepared a series of nano-composites composed of RuO_2 nanoparticles *in situ* loaded on activated multi-walled carbon nanotubes (RuO_2@a-MWCNTs) through hydrolyzing reaction followed by calcination method and used them as cathode catalysts to accelerate the decomposition of Na_2CO_3. Among all catalysts, the RuO_2@a-MWCNTs with appropriate ratio of RuO_2 (49.7 wt%) demonstrated best stability and rate performance in Na-CO_2 batteries, benefiting from both high specific surface area (160.3 m^2/g) and highly dispersed RuO_2 with ultrafine nanostructures (~2 nm). At a limited capacity of 500 mAh/g, Na-CO_2 batteries could afford the operation of over 120 cycles at 100 mA/g, and even at the current density to 500 mA/g, the charge voltage was still lower than 4.0 V after 40 cycles. Further theoretical calculations proved that RuO_2 was the catalytically active center and contributed to the decomposition of Na_2CO_3 by weakening the C=O bond. The synergetic functions of high specific surface (CNTs) and high catalytic activity (RuO_2) will inspire more progress on metal-CO_2 batteries.

Metal-CO_2 batteries have recently attracted plenty of attention because they can utilize greenhouse gas CO_2, along with their high specific energy density [1–4]. Moreover, it is promising to adopt metal-CO_2 batteries as power supplies of future exploration on Mars, in which CO_2 accounts for 95% of the atmosphere [5,6]. Metal Li-CO_2 batteries were firstly investigated and have been widely studied due to both high discharge potential (~2.8 V) and theoretical energy density (1876 Wh/kg) based on the ideal reaction of $4Li+3CO_2 \leftrightarrow 2Li_2CO_3+C$ [7–9]. Plenty of catalysts such as RuO_2, Ru, Mo_2C, NiO have been developed to promote the decomposition of thermodynamically stable discharge products (Li_2CO_3) [10–16]. Considering the limited resource of lithium, sodium with similar physical and chemical properties has also been applied as anode to build Na-CO_2 batteries, in which the theoretical energy density can reach 1125 Wh/kg through the reaction of $4Na+3CO_2 \leftrightarrow 2Na_2CO_3+C$ (~2.35 V) [8,17,18].

Similar with Li-CO_2 batteries, the discharge products of Na-CO_2 batteries (Na_2CO_3) are also hard to decompose, leading to high charge overpotential and poor cycle stability [17–20]. In 2016, with electrolyte-treated multi-wall carbon nanotube (t-MWCNT) as cathode catalyst, we first enabled the rechargeable room temperature Na-CO_2 battery [5]. Since then, a handful of catalysts such as Co_2MnO_x decorated carbon fiber, $ZnCo_2O_4$@CNT, ketjen black carbon or CNT supported ruthenium nanoparticles (Ru@KB or Ru@CNT), have been designed to accelerate the kinetics of the battery [7,18,21,22]. Among them, nano-Ru metal composites stand out with high catalytic characteristics towards Na_2CO_3 decomposition, but their high reactivities undergo the concerns of catalyzing the decomposition of electrolyte [23,24]. As an alternative, RuO_2 catalyst, which is more stable than metal Ru, also exhibits decent electron conductivity. RuO_2@CNTs have been applied as cathode catalysts in Li-CO_2 batteries to facilitate the decomposition of Li_2CO_3 [25,26], which triggers the interest to study the use of ruthenium oxide-based catalysts in Na-CO_2 batteries.

Herein, a series of RuO_2 nanoparticles *in situ* loaded on activated multi-walled carbon nanotubes (RuO_2@a-MWCNTs) have been fabricated through the facile hydrolyzing reaction followed by

* Corresponding author.
E-mail address: zhaoq@nankai.edu.cn (Q. Zhao).

https://doi.org/10.1016/j.cclet.2022.04.003
1001-8417/

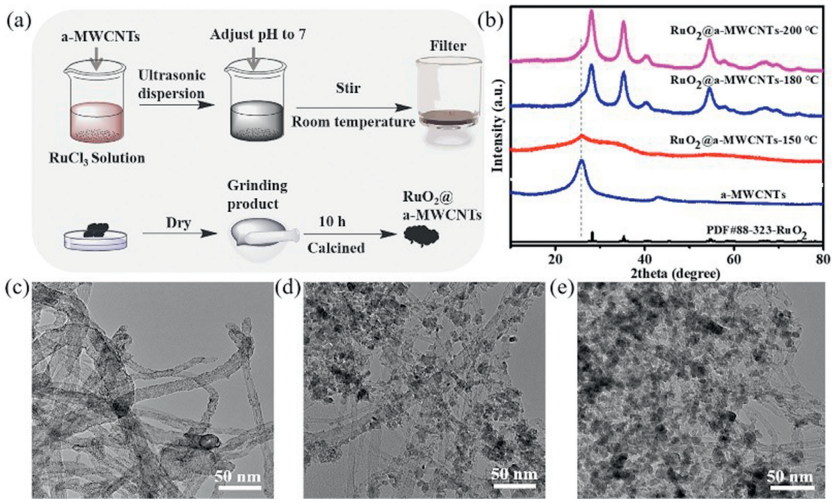

Fig. 1. (a) Schematic diagram of preparing RuO_2@a-MWCNTs composite. (b) XRD patterns of a-MWCNTs, RuO_2@a-MWCNTs-150 °C, RuO_2@a-MWCNTs-180 °C and RuO_2@a-MWCNTs-200 °C. TEM images of (c) RuO_2@a-MWCNTs-150 °C, (d) RuO_2@a-MWCNTs-180 °C and (e) RuO_2@a-MWCNTs-200 °C.

calcination method [27–29] and acted as cathode catalysts to promote the decomposition of Na_2CO_3 in Na-CO_2 batteries. Through optimizing the temperature of calcination and the content of RuO_2, RuO_2@a-MWCNTs prepared at 150 °C with 49.7 wt% RuO_2 demonstrated the best overall performance. The charge/discharge overpotential has been reduced to 1.5 V, in contrast with pure a-MWCNTs catalyst (2.2 V). Further cycling test unveiled the charge voltage of Na-CO_2 batteries with above catalyst were still lower than 4.0 V after 40 cycles at 500 mA/g and after 90 cycles at 100 mA/g under same limited capacity of 500 mAh/g. The results of density functional theory (DFT) calculations showed that RuO_2 was the catalytically active site, and the Ru atoms on RuO_2 and the O atoms on Na_2CO_3 formed covalent bonds, which resulted in the charge transfer on the C=O, elongated the length of C=O bond on the Na_2CO_3, and promoted the decomposition of Na_2CO_3 with low charging overpotential.

Various RuO_2@a-MWCNTs composites were synthesized through the facile hydrolyzing reaction followed by calcination method. The detailed preparation process was shown in Fig. 1a. The precursor powder from the same batch was divided into three parts and calcined at 150 °C, 180 °C, and 200 °C for 10 h to obtain the final products, which were respectively defined as RuO_2@a-MWCNTs-150 °C, RuO_2@a-MWCNTs-180 °C, and RuO_2@a-MWCNTs-200 °C. The results from X-ray diffraction (XRD) indicated that the crystallization increased with the increasing of temperature (Fig. 1b). Pure a-MWCNTs displayed two diffraction peaks at 25.9° and 42.8° that could be assigned to the (002) and (100) planes [30], respectively. When the calcination temperature was 180 °C or higher, the obtained RuO_2 in the composite exhibited decent crystallinity and the XRD patterns matched well with the standard card (PDF#88–323-RuO_2) (Figs. S1 and S2 in Supporting information). For RuO_2@a-MWCNTs-150 °C, the crystallization of RuO_2 was highly suppressed with only one broad diffraction peak centered at around 35°. Meanwhile, RuO_2 nanoparticles were ultrafine and evenly dispersed on carbon nanotubes (Fig. 1c). However, RuO_2 nanoparticles became larger and agglomerated together for RuO_2@a-MWCNTs-180 °C (Fig. 1d) or 200 °C (Fig. 1e).

Considering that the catalysts with highly dispersed and ultrafine characteristics can provide more active sites to accelerate the decomposition of Na_2CO_3 [31], we chose the calcination temperature of 150 °C to further optimize the loadings of RuO_2 nanoparticles (Fig. S3 in Supporting information). The RuO_2 content in

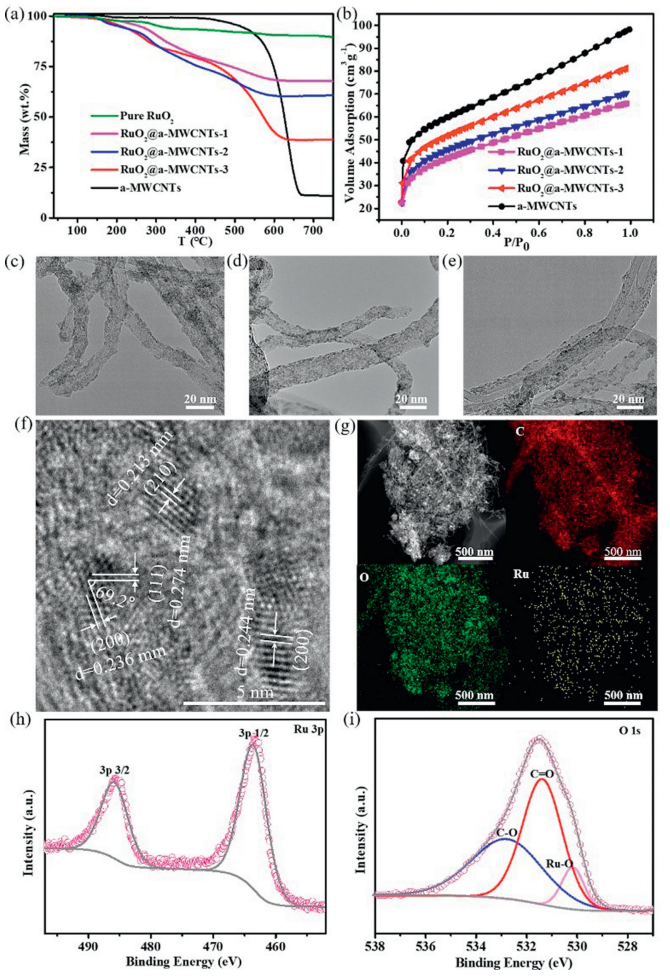

Fig. 2. (a) TG curves of pure RuO_2, RuO_2@a-MWCNTs-1, RuO_2@a-MWCNTs-2, RuO_2@ a-MWCNTs-3 and a-MWCNTs. (b) Nitrogen-adsorption-desorption isotherms of RuO_2@a-MWCNTs-1, RuO_2@a-MWCNTs-2, RuO_2@a-MWCNTs-3 and a-MWCNTs. TEM image of (c) RuO_2@a-MWCNTs-1, (d) RuO_2@a-MWCNTs-2 and (e) RuO_2@a-MWCNTs-3. (f) HRTEM image of RuO_2@a-MWCNTs-2 and (g) C, O, Ru EDX mapping images of RuO_2@a-MWCNTs-2. (h) Ru 3p and (i) O 1s high-resolution XPS spectra of RuO_2@a-MWCNTs-2.

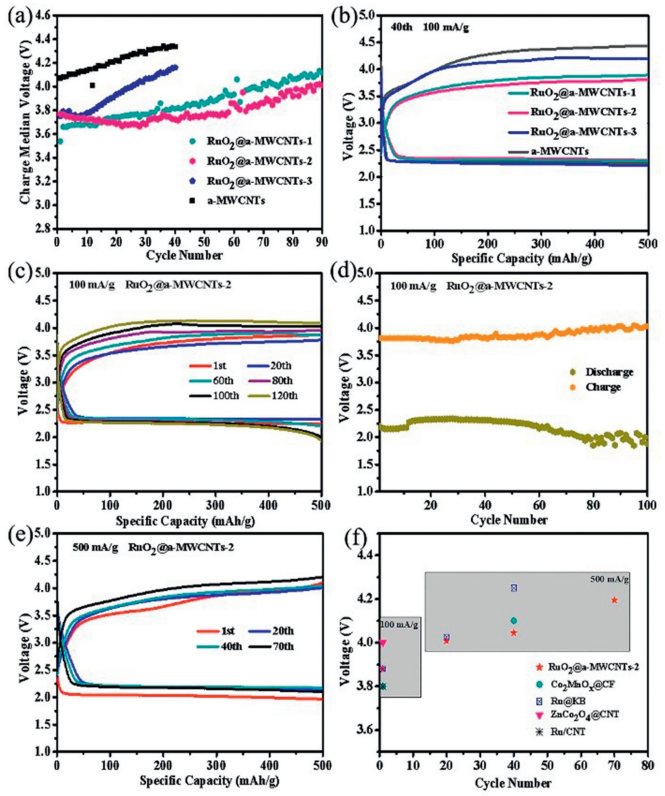

Fig. 3. Performance of Na-CO_2 battery. (a) Median charge voltage over cycles and (b) comparison of the 40th charge−discharge profile of Na-CO_2 battery with RuO_2@a-MWCNTs-1, RuO_2@a-MWCNTs-2, RuO_2@a-MWCNTs-3 and a-MWCNTs cathode. (c) Cycle performance of Na-CO_2 battery using RuO_2@a-MWCNTs-2 cathode with a cutoff capacity of 500 mAh/g at 100 mA/g. (d) The terminal potentials of cycles with RuO_2@a-MWCNTs-2 cathode at 100 mA/g. (e) Cycle performance of Na-CO_2 batteries with a cutoff capacity of 500 mAh/g at 500 mA/g. (f) Comparison of charge voltage of Na-CO_2 batteries with different cathode catalysts.

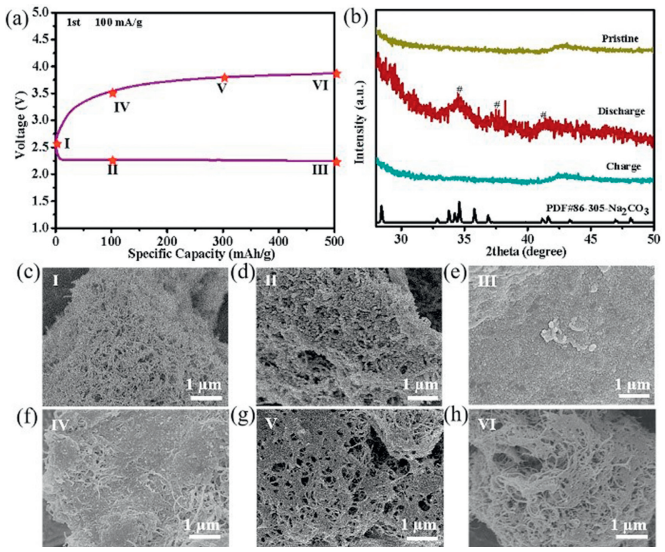

Fig. 4. (a) 1st charge and discharge curve of Na-CO_2 battery with marked points for characterizations. (b) *Ex situ* XRD of RuO_2@a-MWCNTs-2 cathode. *Ex situ* SEM images of RuO_2@a-MWCNTs-2 cathodes: (c) Pristine, (d) discharged 100 mAh/g, (e) discharged 500 mAh/g and (f) recharged 100 mAh/g, (g) recharged 300 mAh/g, (h) recharged 500 mAh/g.

the RuO_2@a-MWCNTs composite was evaluated to be 56.8 wt% (labeled as RuO_2@a-MWCNTs-1), 49.7 wt% (labeled as RuO_2@a-MWCNTs-2), 27.9 wt% (labeled as RuO_2@a-MWCNTs-3) according to the result of thermogravimetric (TG) analysis in air atmosphere (Fig. 2a and Fig. S4 in Supporting information). Based on the N_2-adsorption-desorption measurement, the specific surface area of the composite gradually increased after decreasing the content of RuO_2, which were 147.8, 160.3, 183.8 and 212.8 m^2/g for RuO_2@a-MWCNTs-1, RuO_2@a-MWCNTs-2, RuO_2@a-MWCNTs-3 and pristine a-MWCNTs, respectively (Fig. 2b). Nevertheless, the specific surface area for RuO_2@a-MWCNTs composite was still high enough to accommodate the discharge product of Na-CO_2 batteries with maintained porous structure [27].

We carried out the Transmission electron microscope (TEM), high resolution transmission electron microscope (HRTEM) and energy dispersive X-ray spectroscopy (EDX) to further investigate the distribution of RuO_2 nanoparticles in a-MWCNTs (Figs. 2c-g and Figs. S5-S7 in Supporting information). High RuO_2 content (RuO_2@a-MWCNTs-1) would result in the aggregation of RuO_2 nanoparticles (Fig. 2c and Fig. S5). Reducing the content of RuO_2 nanoparticles (RuO_2@a-MWCNTs-2) enable the uniform distribution of particles (Fig. 2d and Fig. S6). The RuO_2 was more scattered when the content was further reduced (RuO_2@a-MWCNTs-3) (Fig. 2e and Fig. S7). Through calibrating the lattice fringes and the angles between them, the HRTEM image (Fig. 2f) confirmed that the RuO_2 of RuO_2@a-MWCNTs-2 belonged to the cubic phase (PDF#87–726-RuO_2) with average size of about 2 nm. EDX mapping of RuO_2@a-MWCNTs-2 demonstrated Ru and O elements were uniformly distributed (Fig. 2g). X-ray photoelectron spectroscopy (XPS) was adopted to analyze the element valence and bonding states. The XPS high-resolution spectrum of Ru 3p (Fig. 2h) could be fitted to two peaks at 464.0 eV and 486.7 eV, indicating the dominant +4 oxidation state of Ru [31]. The O 1s XPS spectrum could be fitted to three peaks (Fig. 2i). The peak at binding energy of 532.8 eV and 531.4 eV corresponded to C-O and C=O [32,33]. Compared with the XPS spectrum of a-MWCNTs (Fig. S8 in Supporting information), there was an additional peak with a binding energy of 530.2 eV in RuO_2@a-MWCNTs-2, which was related to the Ru-O bond of RuO_2 [34].

The above characterizations suggested that RuO_2@a-MWCNTs-2 took advantages of both high dispersibility and abundant active sites. In order to further study the relationship between the loading ratio of RuO_2 and the catalytic performance, we assembled Na-CO_2 coin cells with RuO_2@a-MWCNTs-1, RuO_2@a-MWCNTs-2, RuO_2@a-MWCNTs-3, or a-MWCNTs as cathode catalysts. The median charging voltage was a straightforward indicator to assess the catalytic capability for Na_2CO_3 decomposition (Figs. 3a-d and Figs. S9-S11 in Supporting information). Obviously, pure a-MWCNTs cathode exhibited the highest potential, exceeding 4 V even on the first lap. RuO_2@a-MWCNTs-3 cathode with lowest content of RuO_2 also demonstrated sharply increased overpotential that exceed 4 V on the 25th lap. Both RuO_2@a-MWCNTs-1 and RuO_2@a-MWCNTs-2 displayed low median charging voltage, while RuO_2@a-MWCNTs-2 demonstrated higher durability and the charging potential was still lower than 4 V after 90 cycles. We attributed it to better dispersed RuO_2 nanoparticles/higher specific surface area than RuO_2@a-MWCNTs-1 and higher RuO_2 ratio than RuO_2@a-MWCNTs-3. Moreover, long cycle test at a limited capacity of 500 mAh/g demonstrated that Na-CO_2 batteries could afford the operation of 70 cycles at 500 mA/g (Fig. 3e), in which the charge voltage was still lower than 4.0 V after 40 cycles at 500 mA/g. The charging voltage only increased by 0.2 V on the 20th lap when the current density increased from 100 mA/g to 500 mA/g (Fig. S12 in Supporting information). Fig. 3f and Fig. S13 (Supporting information) compared the performance of Na-CO_2 battery between RuO_2@a-MWCNTs-2 in this work and cathode catalysts reported in the literature (cut-off capacity was 500 mAh/g).

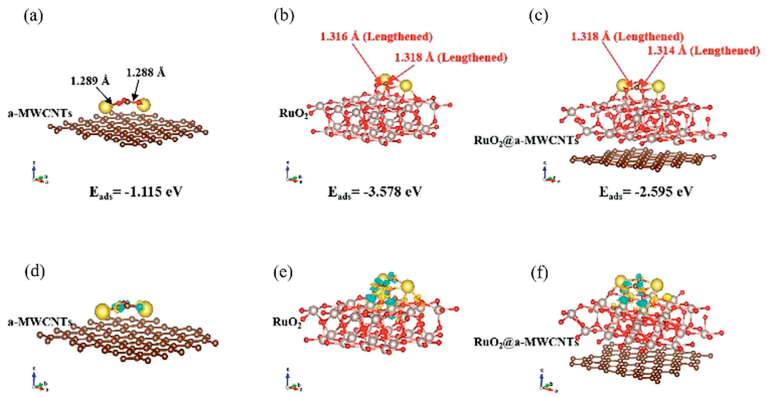

Fig. 5. The interactions between Na_2CO_3 and different cathodes. The optimized configurations, adsorption energies, and C=O bond lengths of Na_2CO_3 on (a) a-MWCNTs, (b) RuO_2 and (c) RuO_2@a-MWCNTs substrates. (d-f) The differential charge density of Na_2CO_3 adsorbed on a-MWCNTs, RuO_2 and RuO_2@a-MWCNTs substrates.

Among all the cathode catalysts, RuO_2@a-MWCNTs-2 catalyst displayed decent charge voltage at low current density (100 mA/g) on the first cycle, and the lowest charge voltage at high current density (500 mA/g) with longest cycling life.

In order to unveil how catalyst contributed to the reaction of Na-CO_2 batteries, *ex-situ* XRD and scanning electron microscope (SEM) characterization have been conducted at different states of charge and discharge (6 state points were marked in Fig. 4a). Na-CO_2 battery with RuO_2@a-MWCNTs-2 catalyst exhibited outstanding reversibility. From the XRD graph (Fig. 4b), three diffraction peaks of Na_2CO_3 at 34.6°, 37.5° and 41.7° were emerged after discharge, and disappeared when charging process was finished. The reversibility was also confirmed by SEM characterization. Plenty of granular products were generated on the carbon nanotube skeleton during the discharge process (Figs. 4c-e and Fig. S14 in Supporting information). The products gradually disappeared, and a porous structure reappeared during the charging process (Figs. 4f-h and Fig. S15 in Supporting information). Even after 20 cycles with a cutoff capacity of 500 mAh/g at 100 mA/g, the RuO_2@a-MWCNTs-2 cathode still showed intriguing catalytic properties for Na_2CO_3 decomposition, sharply contrasting with a-MWCNTs cathode on which a few by-products were accumulated (Fig. S16 in Supporting information). The intriguing results were due to the synergetic functions of CNTs and RuO_2, in which multi-walled carbon nanotubes could provide a huge specific surface area to hold the discharge products, and the RuO_2 nanoparticles could effectively reduce the energy barrier of electrochemical reaction during the charging process to promote the decomposition of Na_2CO_3. Moreover, the oxygen-containing functional groups carried by the activated carbon tubes (Figs. S17-S19 in Supporting information) enabled the uniform dispersion of RuO_2 nanoparticles [6,35,36].

To provide atomic understanding between RuO_2 based catalyst and Na_2CO_3, we further applied the density functional theory (DFT) calculations. Figs. 5a-c and Table S1 (in Supporting information) summarized the configurations of Na_2CO_3 on a-MWCNTs, RuO_2 and RuO_2@a-MWCNTs substrates. The results demonstrated that the adsorption energy of Na_2CO_3 on RuO_2 (−3.578 eV) and RuO_2@a-MWCNTs (−2.595 eV) were more negative than that on a-MWCNTs (−1.115 eV), indicating RuO_2 was the preferred sites to grow Na_2CO_3. Besides, compared with the substrate of a-MWCNTs (1.289 Å, 1.288 Å), the C=O bond of Na_2CO_3 on the substrate of RuO_2 (1.316 Å, 1.318 Å) and RuO_2@a-MWCNTs (1.318 Å, 1.314 Å) were lengthened. The lengthened bond meant that Na_2CO_3 was easier to decompose, proving that RuO_2 nanoparticles were beneficial for the charge process of Na-CO_2 batteries.

The differential charge density was then used to explain that why the C=O bond length was elongated (Figs. 5d-f). Different from a-MWCNTs system, the electron density around the C=O bond of Na_2CO_3 decreased obviously in the RuO_2 and RuO_2@a-MWCNTs system, which was due to the covalent bond that formed between O atoms on the Na_2CO_3 and the Ru atoms on the RuO_2. The newly formed Ru-O interaction directly weakened the C=O bond and thus favored the decomposition of Na_2CO_3. The DFT calculations unambiguously verified that the RuO_2@a-MWCNTs composite cathode catalyst was very effective for fabricating the high stable Na-CO_2 batteries.

In summary, ultra-fine and highly dispersed RuO_2 nanoparticles (~2 nm) loaded on a-MWCNTs have been fabricated and for the first time, acted as cathode catalyst to reduce the charge overpotential and enhance the reversibility of Na-CO_2 batteries. a-MWCNTs with O-rich groups facilitated the dispersion of RuO_2 and RuO_2 promoted Na_2CO_3 decomposition by weakening the C=O bond of Na_2CO_3, which together contributed to build the Na-CO_2 batteries with long cycle life (>120 cycles) and low charge potential (<4.0 V up to 90 cycles). This work provides a general way to promote the decomposition of Na_2CO_3. With rational designation, more composite catalysts with advanced conductive host such as graphene, porous carbons, MXene can be prepared to further enhance the properties of metal-CO_2 batteries.

Declaration of competing interest

The authors declare that they have no known competing financial interests or personal relationships that could have appeared to influence the work reported in this paper.

Acknowledgments

This work was supported by the National Natural Science Foundation of China (Nos. 52001170, 21835004), the National Key R&D Program of China (Nos. 2017YFA0206700, 2021YFB2500300) and the Natural Science Foundation of Tianjin (No. 20JCQNJC02060).

Supplementary materials

Supplementary material associated with this article can be found, in the online version, at doi:10.1016/j.cclet.2022.04.003.

References

[1] J. Sun, Y. Lu, H. Yang, et al., Research 2018 (2018) 6914626.
[2] X. Mu, H. Pan, P. He, et al., Adv Mater. 32 (2019) e1903790.

[3] Y. Hou, J. Wang, L. Liu, et al., Adv. Funct. Mater. 27 (2017) 1700564.
[4] S. Shen, C. Han, B. Wang, et al., Chin. Chem. Lett. 33 (2022) 3721–3725.
[5] X. Hu, J. Sun, Z. Li, et al., Angew. Chem. Int. Ed. 55 (2016) 6482–6486.
[6] Y. Lu, Y. Cai, Q. Zhang, et al., Chem. Sci. 10 (2019) 4306–4312.
[7] S. Thoka, C.M. Tsai, Z. Tong, et al., ACS Appl. Mater. Interfaces 13 (2021) 480–490.
[8] S. Yang, Y. Qiao, P. He, et al., Energy Environ. Sci. 10 (2017) 972–978.
[9] S. Ma, Y. Lu, H. Yao, et al., Chin. Chem. Lett. 33 (2022) 2933–2936.
[10] Y. Dong, S. Li, S. Hong, L. Wang, B. Wang, Chin. Chem. Lett. 31 (2020) 635–642.
[11] X. Zhang, C. Wang, H. Li, et al., J. Mater. Chem. A 6 (2018) 2792–2796.
[12] Y. Xing, Y. Yang, D. Li, et al., Adv. Mater. 30 (2018) e1803124.
[13] C. Yang, K. Guo, D. Yuan, et al., J. Am. Chem. Soc. 142 (2020) 6983–6990.
[14] Z. Zhang, Q. Zhang, Y. Chen, et al., Angew. Chem. Int. Ed. 54 (2015) 6550–6553.
[15] K. Chen, G. Huang, J.L. Ma, et al., Angew. Chem. Int. Ed. 59 (2020) 16661–16667.
[16] R. Pipes, A. Bhargav, A. Manthiram, Adv. Energy Mater. 9 (2019) 1900453.
[17] Z. Zheng, C. Wu, Q. Gu, et al., J. Energy Environ. Mater. 4 (2021) 158–177.
[18] S. Thoka, Z. Tong, A. Jena, et al., J. Mater. Chem. A 8 (2020) 23974.
[19] Z. Zhang, X.G. Wang, X. Zhang, et al., Adv. Sci. 5 (2018) 1700567.
[20] L. Qie, Y. Lin, J.W. Connell, et al., Angew. Chem. Int. Ed. 56 (2017) 6970–6974.
[21] L. Guo, B. Li, V. Thirumal, et al., Chem. Commun. 55 (2019) 7946–7949.
[22] C. Fang, J. Luo, C. Jin, et al., ACS Appl. Mater. Interfaces 10 (2018) 17240–17248.
[23] X. Xing, I. Kimihiko, K. Yoshimi, Electrochim. Acta 261 (2018) 323e329.
[24] S. Ma, Y. Wu, J. Wang, et al., Nano Lett. 15 (2015) 8084–8090.
[25] Z. Xie, X. Zhang, Z. Zhang, et al., Adv. Mater. 29 (2017) 1605891.
[26] S. Bie, M. Du, W. He, et al., ACS Appl. Mater. Interfaces 11 (2019) 5146–5151.
[27] Y. Eda, Y. Chihiro, Y. Keisuke, et al., Nano Lett. 13 (2013) 4679–4684.
[28] P. Xua, C. Chen, J. Zhu, et al., J. Electroanal. Chem. 842 (2019) 98–106.
[29] Z. Jian, P. Liu, F. Li, et al., Angew. Chem. Int. Ed. 53 (2014) 442–446.
[30] R. Wang, X. Zhang, Y. Cai, et al., Nano Res. 12 (2019) 2543–2548.
[31] S.-.M. Xu, Z.-.C. Ren, X. Liu, et al., Energy Storage Mater. 15 (2018) 291–298.
[32] M. Chuai, J. Yang, M. Wang, et al., eScience 1 (2021) 178–185.
[33] S. Kundu, Y. Wang, W. Xia, et al., J. Phys. Chem. C 112 (2008) 16869–16878.
[34] X. Gao, J. Chen, X. Sun, et al., ACS Appl. Nano Mater. 3 (2020) 12269–12277.
[35] A. Huang, Y. Ma, J. Peng, et al., eScience 1 (2021) 141–162.
[36] J.G. Zhou, H.T. Fang, Y.F. Hu, et al., J. Phys. Chem. C 113 (2009) 10747–10750.